2018

Two Decades of Advancement in Process Simulation Testing of Ballast Strength, Deformation, and Degradation

Buddhima Indraratna
University of Wollongong, indra@uow.edu.au

Ngoc Trung Ngo
University of Wollongong, trung@uow.edu.au

Sanjay Nimbalkar
University of Technology Sydney, sanjayn@uow.edu.au

Cholachat Rujikiatkamjorn
University of Wollongong, cholacha@uow.edu.au

Two Decades of Advancement in Process Simulation Testing of Ballast Strength, Deformation, and Degradation

Abstract

This paper describes salient features of a set of large-scale ballast testing equipment developed at the University of Wollongong, Australia, and how the test results and research outcomes have contributed to transforming tracks in the Australian heavy haul and commuter networks, particularly with regards to the strength, deformation, and degradation of ballast. Ideally, ballast assemblies should be tested in prototype scale under actual loading conditions. This is because a reduction in particle sizes for testing in smaller equipment can reduce the internal angle of friction (shearing resistance) of the granular assembly in a macro sense, and the angularity of the particles in a micro sense, and hence the volumetric changes during the shearing process. In response to the worldwide lack of proper test facilities for ballast, the University of Wollongong has, since the early 1990s, designed and built a number of large-scale process simulation triaxial testing rigs. They are all custom made to minimize any boundary effects and also to evaluate the deformation and degradation of ballast, particularly the size, shape, and origin of aggregates used as ballast in Australian tracks. This triaxial process simulation equipment was originally used to characterize the behavior of coarse aggregate used for state railway standards for monotonic loading, but since then it has been fitted with dynamic actuators to simulate actual track conditions involving the true cyclic loading nature while also capturing the wheel-rail dynamics that correspond to high-speed commuter rail and fast heavy-haul operations. These tests invariably demonstrated completely different stress-strain and volumetric characteristics of ballast compared to conventional static or monotonic testing of the same test specimens.

Disciplines

Engineering | Science and Technology Studies

Paper Title: **Two Decades of Advancement in Process Simulation Testing of Ballast - Strength, Deformation, and Degradation**

Authors: Buddhima Indraratna[1], Ngoc Trung Ngo[2], Sanjay Nimbalkar[3], and Cholachat Rujikiatkamjorn[4],

[1]*Distinguished Professor, *[2]*Research Fellow, *[4]*Associate Professor, Centre for Geomechanics and Railway Engineering, Faculty of Engineering and Information Sciences, ARC Centre of Excellence for Geotechnical Science and Engineering University of Wollongong, Wollongong, NSW 2522.*

[3]*Lecturer, University of Technology Sydney. Email: Sanjay.Nimbalkar@uts.edu.au*

Corresponding authors: Prof Indraratna: Email: indra@uow.edu.au; Dr Ngoc Trung Ngo: Email: trung@uow.edu.au

Abstract

This paper describes salient features of a set of large-scale ballast testing equipment developed at University of Wollongong (UOW), Australia, and how the test results and research outcomes have contributed to transforming tracks in the Australian heavy haul and commuter networks, particularly with regards to the strength, deformation, and degradation of ballast. Ideally, ballast assemblies should be tested in prototype scale under actual loading conditions. This is because a reduction in particle sizes for the testing in smaller equipment can reduce the internal angle of friction (shearing resistance) of the granular assembly in a macro sense, and the angularity of the particles in a micro sense, and hence the volumetric changes during the shearing process. In response to the worldwide lack of proper test facilities for ballast, UOW has, since the early 1990s, designed and built a number of large-scale process simulation triaxial testing rigs. They are all custom made to minimize any boundary effects and also evaluate the deformation and degradation of ballast, particularly the size, shape and origin of aggregates used as ballast in Australian tracks. This triaxial process simulation equipment was originally used to characterize the behavior of coarse aggregate used for state railway standards for monotonic loading, but since then it has been fitted with dynamic actuators to simulate actual track conditions involving the true cyclic loading nature, whilst also capturing the wheel-rail dynamics which correspond to high-speed commuter rail and fast heavy haul operations. These tests invariably demonstrated completely different stress-strain and volumetric characteristics of ballast compared to conventional static or monotonic testing of the same test specimens.

Keywords: Ballast Testing, Confining Pressure, Particle Breakage, Triaxial Test.

1.   Introduction

Railroads form the largest worldwide network catering for quick and safe, public and freight transportation. In order to compete with the other modes of transportation and meet the ever growing demand of public and freight transport, railway industries face challenges to improve their efficiency and decrease the cost of maintenance and infrastructure [1-3]. The need to remain competitive with other means of transportation compels railway organizations to become even more efficient and also decrease the costs of maintenance and infrastructure. In spite of recent advances in rail geotechnics, choosing ballast that is suitable for rail track foundation is very important because aggregates progressively deteriorate and break down under heavy cyclic loading [4-6]. The degradation of ballast is influenced by factors including the amplitude and number of load cycles, gradation of aggregates, track confining pressure, and the angularity and fracture strength of individual grains. The cost of track maintenance can be significantly reduced if the geotechnical behavior of rail substructure, particularly the ballast layer is better understood [2].

Ballast forms the largest component of a rail track by weight and volume. Ballast materials usually include dolomite, rheolite, gneiss, basalt, granite and quartzite [7]; and consists of medium to coarse gravel sized aggregates (10 - 60 mm) with a smaller percentage of cobble-sized particles [1, 8]. Good quality ballast should have angular particles, a high specific gravity, high shear strength, high toughness and hardness, high resistance to weathering, a rough surface, and a minimum of hairline cracks [9-13]. The main functions of ballast are to distribute and dampen the loads received from sleepers, produce lateral resistance, and provide rapid drainage. It could be argued that ballast for high load bearing characteristics and maximum track stability should be angular, well graded, and compact so that it reduces drainage. Accordingly, the Centre for Geomechanics and Railway Engineering (CGRE) at the University of Wollongong is founded under the auspices of the Cooperative Research Centre for Railway Engineering and Technologies (RAIL-CRC), and in collaboration with other railway organizations in Australia, has initiated an extensive research program to study the behavior of rail track under dynamic impact and cyclic loading. The following investigations are already complete, so the main findings of this study are presented here: (i) studying the mechanical behavior of ballast under monotonic and cyclic loading; (ii) examining the effect that the particle size and shape, confining pressure and load frequency on ballast's shear strength, deformation, and degradation, based on static and dynamic tests using the large-scale cylindrical triaxial apparatus; (iii) quantifying ballast breakage and fouling; and (iv) the use of geosynthetics and rubber mats in improved performance of ballast.

2.   Prototype testing and experimental simulations

The conventional triaxial apparatus is a versatile method for obtaining the deformation and strength of coarse- and fine-grained materials in the laboratory, but the discrepancy between the actual particle shape and sizes in the field and the reduced particle sizes adopted in conventional laboratory equipment leads to

inaccurate load-deformation responses and failure modes. These inaccurate measurements are the result of the inevitable size dependent dilation and different mechanisms of particle crushing [14]; this means that testing coarse aggregates in conventional apparatus can give misleading results because of disparities between particle and equipment size, but as the ratio of the specimen to maximum particle size exceeds 6, the effects due to equipment boundaries can be ignored [15]. To mitigate these size dependent issues, large-scale facilities for testing ballast have been designed and built at the University of Wollongong over the last two decades, as shown in Figure 1. As expected, these testing facilities provide more realistic information on the stress–strain and degradation behavior of ballast. Further details of the components of this apparatus and the measuring techniques can be found elsewhere [16-23], among others.

A large-scale triaxial testing apparatus (Figure 1a) which can accommodate sample of 300 mm diameter and 600 mm high was used for testing railway ballast. The apparatus consist of six main parts: the triaxial chamber, the vertical loading unit, the oil reservoir and pump, the servo-control unit and the digital data acquisition system. The deviator stress was applied by a dynamic actuator capable of frequencies up to 60 Hz at load amplitudes of 150 kN. Each specimen was subjected to a given loading frequency, and the loading was suspended after 500 000 cycles, irrespective of the axial strain achieved. Before and after loading, the ballast was passed through the set of 12 standard sieves (2.36–53 mm) at least twice to ensure accurate breakage estimation. A large-scale process simulation testing apparatus (PSTA) has been designed and built to study the response of ballast track components under realistic cyclic loading (Fig. 1b); it was the first of its kind in the world when used in the early 1990s. This PSTA can accommodate specimens 800 mm long, 600 mm wide, and 600 mm high; these dimensions were selected to mimic a typical unit cell section of Australian standard gauge tracks [24, 25]. Furthermore, this PSTA is a true triaxial apparatus because three independent principal stresses can be applied in three mutually orthogonal directions and it can apply a 100 kN dynamic actuator load with frequency of up to 40 Hz to simulate heavy haul trains with a 40 ton axle load travelling at up to 300 km/hour. A large permeameter has also been designed (Figure 1c) to measure the hydraulic conductivity of ballast contaminated with fouling materials such as coal and subgrade mud [19]. The size of this apparatus is 0.5 m in diameter and 1 m in height. A filter membrane was placed above a coarse granular layer (prepared from coarser ballast aggregates) while still maintaining a free drainage boundary to prevent fouling material flowing out. The thickness of ballast layer in Australian rail track varies between 300 mm and 500 mm. In view of this, 500 mm thick ballast layer was used to determine the permeability of fouled ballast. The test specimen was placed above the filter membrane and compacted in four equal layers to represent a typical field density of 1600 kg/m^3. Commercial kaolin (plastic and liquid limits are 26.4 % and 52.1 % respectively) was used to simulate the clay fouling. Predetermined amount of fouling corresponding to different degree of fouling was mixed with ballast and compacted to gain similar density of ballast, so that

the voids of the ballast were kept constant throughout the test series. High-capacity drop-weight impact testing equipment (Figure 1d) was also used to examine the effects of rubber mats in the attenuation of dynamic impact loads and subsequent mitigation of ballast degradation [26]. The impact apparatus consists of a free-fall hammer of 5.81 kN weight that can be dropped from a maximum height of 6 m, guided through rollers on the vertical columns fixed to the strong floor. These drop heights and drop mass are selected to produce dynamic stresses in the range of 400-600 kPa, simulating and a typical wheel-flat and dipped rail joint. Impact loads are monitored by a dynamic load cell (capacity of 1,200 kN), mounted on the drop hammer and connected to a computer controlled data acquisition system [27]. An accelerometer is attached on the top surface of ballast assembly to measure accelerations during impact tests. A summary of the key findings determined at the University of Wollongong when this equipment was used to test ballast is reviewed in the following sections.

It is also noted that there have been several limitations of these testing apparatus, including: (i) these equipment cannot simulate the moving load that actually happens in the field; (ii) these apparatus have a limitation in terms of simulating high number of load cycles due to boundary constraints; (iii) some boundary effects will affect testing results, in particular for large-size ballast particles.

3.   Ballast behavior - monotonic and cyclic testing

Several researches have been presented on the effects that the loading characteristic (i.e. monotonic or cyclic loads) has on the stress and strain of railway ballast [e.g. 14, 17, 28]. It is noted that the current standards for railway ballast, e.g. Standards Australia [29] specify the physical and durability required by the parent rock, but do not properly evaluate its performance under in situ track conditions [30]. Ballast used for laboratory test conducted at the UOW is latite basalt (i.e. a dark-coloured volcanic (igneous) rock containing mainly feldspar, plagioclase, and augite) was commonly used as railway ballast in New South Wales, Australia. Figure 2 shows the particle size distribution adopted in the laboratory tests carried out at the UOW, and which is representative of current industry practice.
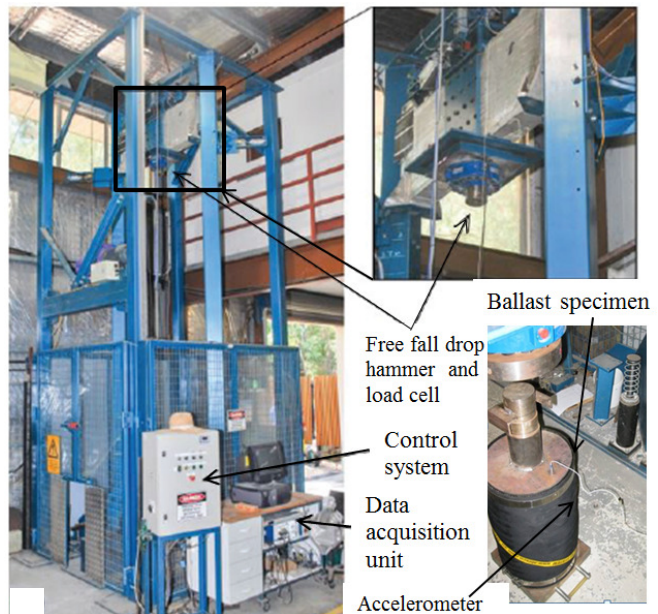
(a) Large-Scale Triaxial Apparatus
(after Indraratna *et al.* [14])
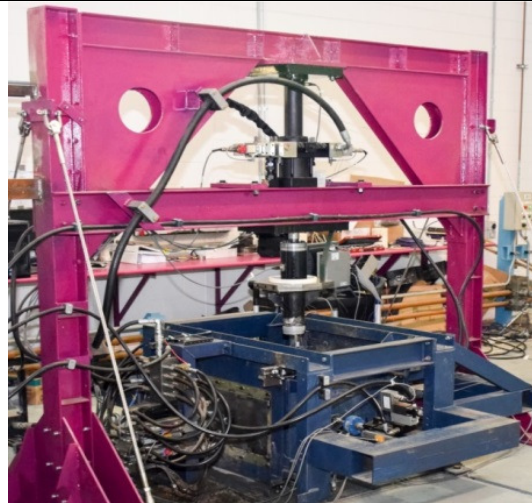
(b) Process Simulation Testing Apparatus (PSTA)
(after Indraratna *et al.* [20])

(c) Large-scale Permeability Test Apparatus
(photo taken at HighBay lab – UOW)

(d) Impact Testing Apparatus
(after Remennikov and Kaewunruen [26])

Figure 1. Selected large-scale ballast testing equipment at the University of Wollongong, Australia
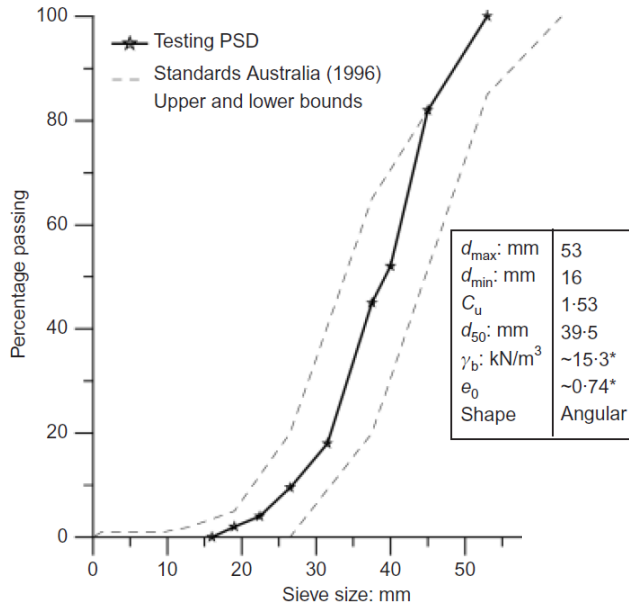
Figure 2. Particle size distribution of ballast tested in the laboratory (after Indraratna *et al.* [14], with permission from ASCE)

3.1 Stress-strain behavior of ballast

A series of isotropically consolidated drained triaxial tests were conducted on fresh ballast using large-scale cylindrical triaxial apparatus (Fig. 1a) under varying confining pressures. The variations of deviator stresses ($q = \sigma'_1 - \sigma'_3$) and volumetric strains ($\varepsilon_v = \varepsilon_1 + 2\varepsilon_3$) with the corresponding shear strains [$\varepsilon_s = 2/3(\varepsilon_1 - \varepsilon_3)$] for the fresh ballast under monotonic triaxial loading are shown in Figure 3. The parameters σ'_1 and σ'_3 represent the major and minor principal effective stresses and the corresponding strains are denoted by ε_1 and ε_3, respectively. It is clearly seen that the shear behavior of the ballast is non-linear and an increase in confining pressure results in increases the deviator stress, as expected. At low confinement (≤ 100 kPa), the volume of ballast increases (i.e. dilation, represented by negative ε_v) during drained shearing. Higher confining pressure tends to shift the overall volumetric strain towards contraction (i.e. ε_v becomes positive). A state of peak deviator stress ($\sigma'_1 - \sigma'_3)_p$, can be considered as 'failure' for ballast. At low confining pressure, a peak deviator stress (i.e. failure) is pronounced, followed by a post–peak strain softening associated with the volume increase.

The stress-strain response of ballast under repeated cyclic loading carried out in the prismoidal triaxial chamber at different intervals of cyclic loading is shown in Figure 4. It indicates that during the initial stage of cyclic loading (cycles 1–5), the mean slope of the hysteresis loop increases rapidly with the higher number of cycles. It is seen that with the increase in vertical load and associated deformation during the first cycle of repeated load, the aggregates re-arranged themselves, therefore, the void ratio decreased, which resulted in

6

higher stiffness. The unloading path indicates a non-linear resilient behaviour with some strain recovery, while the plastic strain keeps significant after unloading was completed. The re-loading path clearly becomes almost linear with increased strain, while the subsequent unloading path remains non-linear.
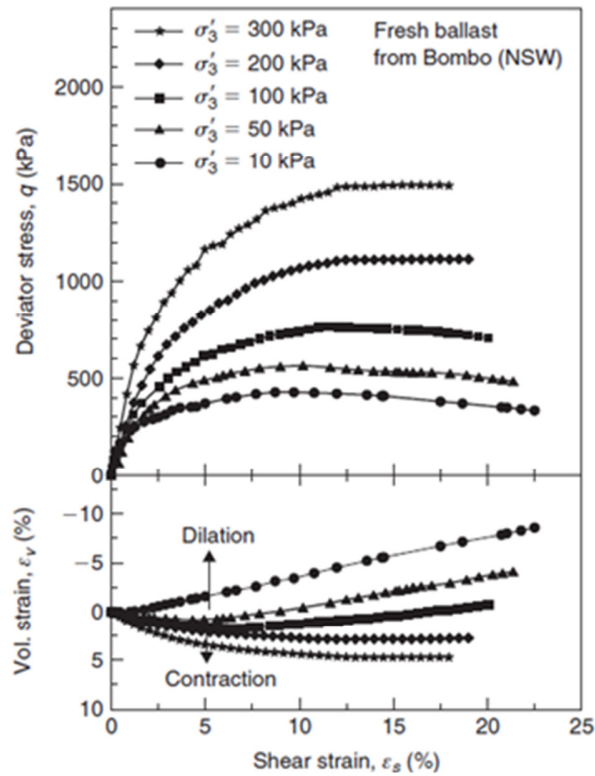

Figure 3. Stress-strain and volume change behavior of fresh ballast measured from large-scale triaxial apparatus (after Indraratna *et al.* [2])
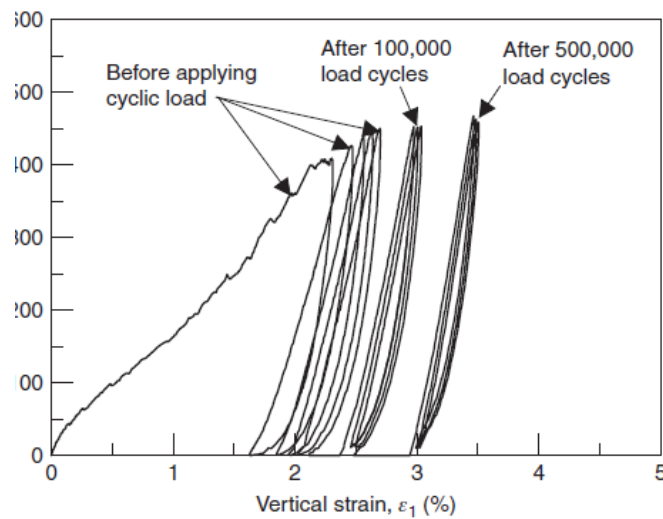

Figure 4. Stress-strain plots in repeated load test at various stages of cyclic loading (after Indraratna *et al.*[2])

3.2   Shear Strength

Since the shear strength of granular materials is generally considered to change linearly with the applied stress, the Mohr-Coulomb theory is usually adopted to describe the shear behavior of ballast. Previous research carried out by Indraratna et al. [31] and Ramamurthy [32], among others, indicates that when soils at high stresses and rocks at low normal stresses are tested, a non-linear shear strength response is obtained, so one value of the cohesion intercept c and the angle of shearing resistance ϕ cannot precisely represent the failure envelopes corresponding to the entire range of stresses. Indraratna et al. [14] proposed the use of a non-linear strength envelope obtained while testing granular media at low normal stresses; this non-linear shear stress envelope is represented by the equation:

$$\frac{\tau_f}{\sigma_c} = m \left(\frac{\sigma_n'}{\sigma_c}\right)^n \tag{1}$$

where, τ_f is the shear stress at failure, σ_c is the uniaxial compressive stress of the parent rock determined from the point load test, m and n are dimensionless constants, and σ_n' is the effective normal stress. The non-linearity of the stress envelope is governed by the coefficient n. For the usual range of confining pressures (below 200 kPa) for rail tracks, n takes values in the order of 0.65 - 0.75. A large-scale cylindrical triaxial apparatus which can accommodate 300m diameter by 600mm high ballast assemblies, has been designed by Indraratna et al. (1998) to validate the non-linearity of shear stress. The results of this study associated with latite basalt in a normalized form are shown in Figure 5 with data presented by other researchers [9, 10, 11].
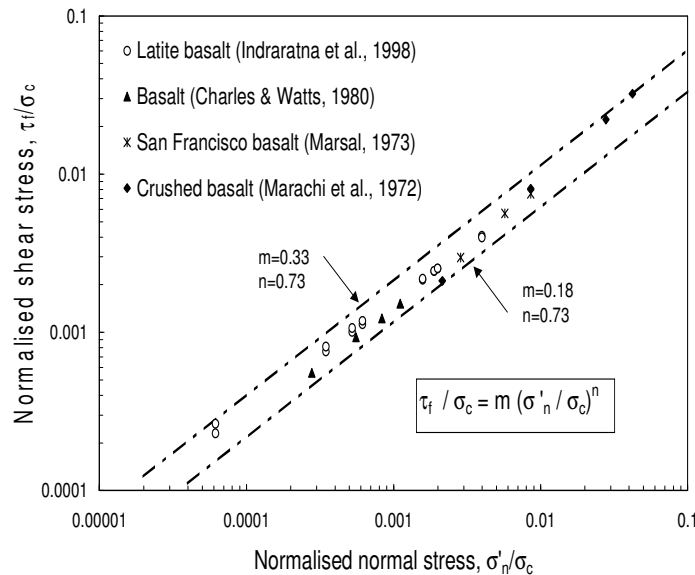

Figure 5. Normalised shear strength for latite basalt aggregates (after Indraratna et al. [14], with permission from ASCE)

8

3.3 Volumetric behavior of ballast under monotonic and cyclic loading

Following extensive laboratory tests, the volumetric strains measured at different confining pressures are shown in Figure 6 where dilation (volume increase) occurred in the ballast samples for most confining pressures under monotonic loads. Although similar ballast materials were also tested in the same large-scale triaxial apparatus, they all exhibited different volumetric strain responses under different loading conditions. Those ballast assemblies which underwent cyclic loads (i.e. confining pressure higher than 30 kPa) experienced pronounced compression, possibly due to the reorientation and rearrangement of particles which occurs during cyclic loading generates a denser (compressing) or looser (dilating) packing assembly. Those specimens subjected to low confinement exhibited purely dilative behavior, whereas the reverse occurred for assemblies with higher confining pressures.

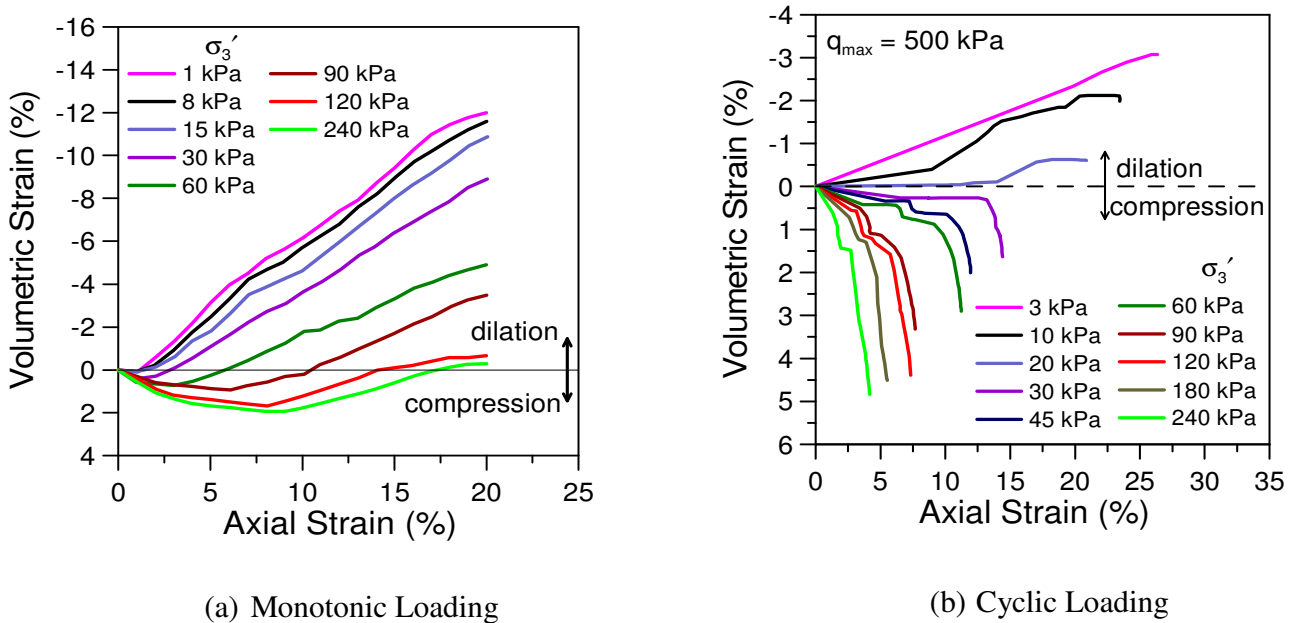(a) Monotonic Loading

(b) Cyclic Loading

Figure 6. Volumetric strains of ballast tested under monotonic and cyclic loading (after Indraratna *et al.* [14], Lackenby *et al.* [17], with permission from ASCE)

3.4 Effect of confining pressure

Although the influence that the confining pressure has on various geotechnical structures is an important design criteria, it is commonly underestimated in conventional rail track design and construction. A series of cyclic triaxial tests have been carried out at the UOW to investigate how confining pressures affect ballast under cyclic loading [17, 33], among others. Ballast specimens were prepared to the recommended gradation (i.e. $d_{50} = 38.5$ mm, $C_u = 1.54$. $e_o = 0.76$; where d_{50} is the diameter of ballast corresponds to 50% finer in the particle size distribution curve and C_u is the coefficient of uniformity), and then tested under effective confining pressures (σ_3') ranging from 1 to 240 kPa with $q_{max} = 500$ kPa.

Figure 7a shows the results of confining pressure $(\sigma_3{'})$ on the axial and volumetric strains of ballast measured at the end of 500,000 cycles; here the axial strains decrease with an increasing confining pressure and the ballast assemblies dilate at a low confining pressure $(\sigma_3{'} < 30)$, but become progressively more compressive as the confining pressure increases from 30 to 240 kPa. The effect of confining pressure on particle breakage is shown in Figure 7b, where breakage is divided into three regions: (I) a dilatant unstable degradation zone (DUDZ); (II) an optimum degradation zone (ODZ); and (III) a compressive stable degradation zone (CSDZ). The data shows that the specimens are subjected to rapid and considerable axial and expansive radial strains that result in an overall volumetric increase or dilation at a low confining pressure in the DUDZ region $(\sigma_3{'} < 30$ kPa). Due to the low confining pressures in this zone, the ballast particles have limited particle-to-particle areas of contact, but as the confining pressure increases to the ODZ region $(\sigma_3{'} = 30 - 75$ kPa), the rate of axial strain decreases due to an apparent increase in stiffness, and the overall volumetric behavior is slightly compressive [17]. Therefore the particles in this region are held together in an optimum array with enough lateral confinement to provide an optimum distribution of contact stress and increased areas of inter-particle contact which decrease the risk of particle breakage. As $\sigma_3{'}$ increases further in the CSDZ region $(\sigma_3{'} > 75$ kPa), the particles rub against each other, which limits their sliding and rolling but significantly increases their breakage. Increasing confinement decreases track settlement while increasing track stability and stiffness (resilient modulus) under cyclic loading, leading to greater track stability and passenger comfort. In summary, this study has found the optimum confining pressure based on loading and track conditions and suggests that track confinement can be increased by decreasing the spacing of sleepers, increasing the height of shoulder ballast, including a geosynthetic (i.e. geogrids, geocomposite) at the ballast-subballast interface, widening the sleepers at both ends, and using intermittent lateral restraints at various parts of the track [2, 34].

3.5   Influence of train frequency on ballast degradation

The influence of frequency on the deformation and degradation of ballast during cyclic loading has been studied using the large scale cyclic triaxial equipment designed and built at the University of Wollongong [33]. Latite ballast was thoroughly cleaned, dried, and sieved through a set of sieves to prepare the grain size distribution in accordance with the Australian standard [19]. These specimens were then placed inside a 5 mm thick Neoprene rubber membrane in four separate layers to a density of 1510 kg/m^3, and then isotropically consolidated to a confining pressure $(\sigma_3{'})$ of 10, 30, and 60 kPa. Frequencies varying from 5 Hz to 60 Hz were used to simulate train speeds from about 40 to 400 km/h, and maximum cyclic deviator stresses $(q_{max,cyc})$ of 230 and 370 kPa represented axle loads of 25 and 40 tonnes, respectively.

Sun *et al.* [33] stated that there are four regimes of permanent deformations based on the cyclic loads applied: (a) a zone of elastic shakedown where no plastic strain accumulates, (b) a zone of plastic shakedown characterized by a steady-state response and a small accumulation of plastic strain, (c) a ratcheting zone with a constant accumulation of plastic strain, and (d) a plastic collapse zone where plastic strains accumulate rapidly and failure occurs in a relatively short time. This study noted three different deformation mechanisms, as show in Figure 8, in response to frequency of loading; in Range I: plastic shakedown at $f \leq$ 20 Hz; in Range II: plastic shakedown and ratcheting at 30 Hz $\leq f \leq$ 50 Hz; in Range III: plastic collapse at $f \geq$ 60 Hz. The influence of frequency (f) and maximum cyclic deviator stress ($q_{max,cyc}$) on ballast breakage were mesured using the BBI proposed by Indraratna *et al.* [18] for different values of f and $q_{max,cyc}$; during cyclic testing the latite basalt ballast experienced degradation which corresponds to different ranges of deformation. Particle degradation in Range I ($f \leq$ 30 Hz) took the form of attrition of asperities and corner breakage, as shown in Figure 9a, but as the frequency increased (30 < f < 60 Hz) in Range II, there is a high degree of attrition resulting from increased vibration (Figure 9b and Figure 9c). At a very high frequency ($f \geq$ 60 Hz) in Range III, the coordination number decreased considerably, which would induce the particle splitting shown in Figure 9d.
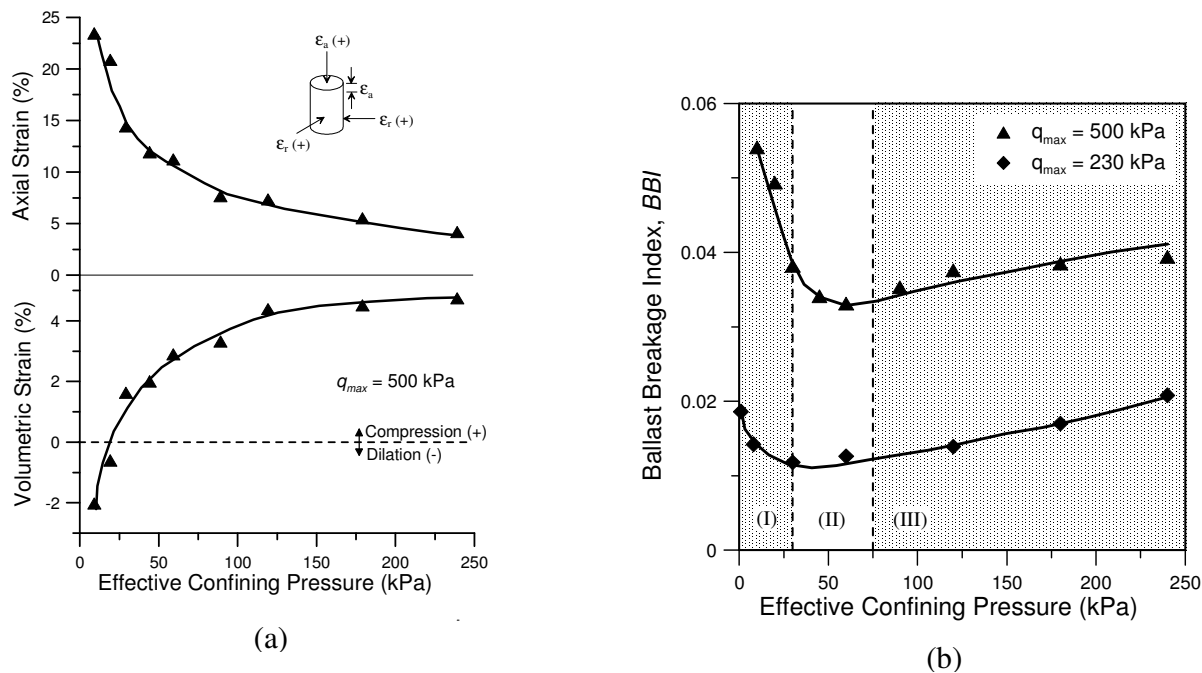

(a)

(b)

Figure 7. Effect of confining pressures on: (a) axial and volumetric strains; (b) particle degradation (after Lackenby *et al.* [17)
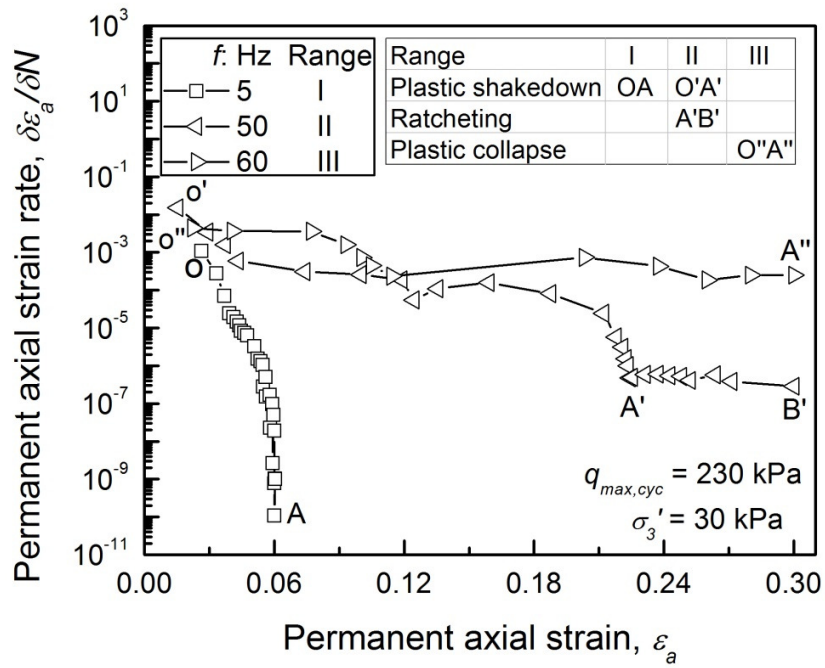
Figure 8. Permanent axial strain rate versus permanent axial strain for selected specimens (after Sun *et al.* [33], with permission from ASCE)
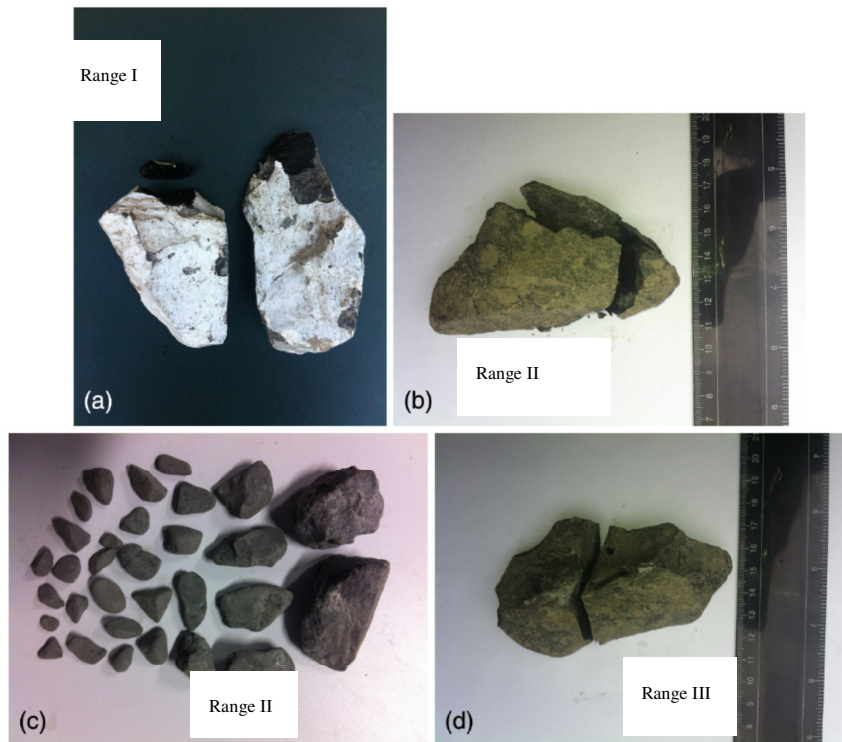

Figure 9. Examples of ballast degradation: (a) corner breakage; (b) particle splitting; (c) high degree attrition of asperities; (d) particle splitting (Sun *et al.* [33], with permission from ASCE)

4.   Effects of particle angularity - size and shapes

The size and shapes of aggregates has long been considered as essential factors that affect the performance of ballast, but only limited in-depth studies have examined these effects [36-39]. Ngo *et al.* [6] conducted discrete element modelling study for railway ballast and they indicated that irregularly-shaped ballast particles should be adequately modelled to capture a correct stress-strain behavior of ballast. Sieving is one of the approaches applied to quantify particle size but it cannot quantify the actual shape of particles; this is why an image-based analysis is more appropriate [35]. However, most previous studies are based on two dimensional (2D) or approximate three dimensional (3D) scanning which cannot really explain the form of individual particles [36-38]. This section summarizes reports from recent studies on a 3D assessment of particle size and shape where a 3D laser scanner has been utilized (Figure 10). To facilitate 3D analysis, a modified index called 'ellipsoidness' *E* is proposed by Sun *et al.* [40] and is shown in Figure 11.

The distribution of ellipsoidness (Figure 11a) presents a greater variation between different sieve intervals than roundness because mean ellipsoidness experiences a very slight reduction as particle size increases, which indicates there should be more angularity in the larger particles (Figure 11b). Although there may be small differences in the surface irregularity of each sieve interval, they would still have a significant effect on the mechanical response of granular materials [41]. To effectively quantify the amount of fragmentation within the representative volume of randomly compacted crushable granular materials, Hardin [42] introduces a relative breakage index based on the relative position of the current cumulative distribution from (i) an initial cumulative distribution, and (ii) an arbitrary cut-off value of 'silt' particle size of 0.074 mm.
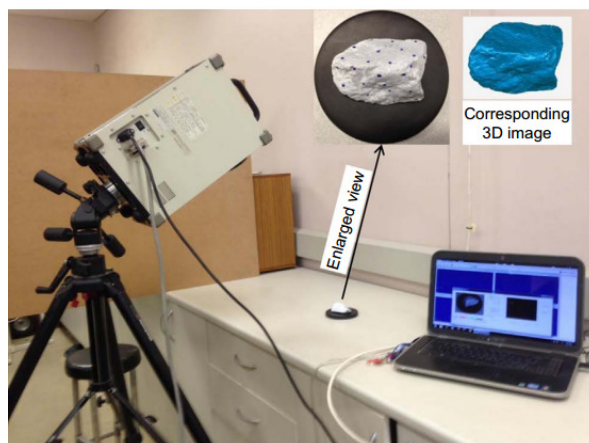

Figure 10. Test set up for 3D assessment of particle size and shape (after Sun *et al.* [40])
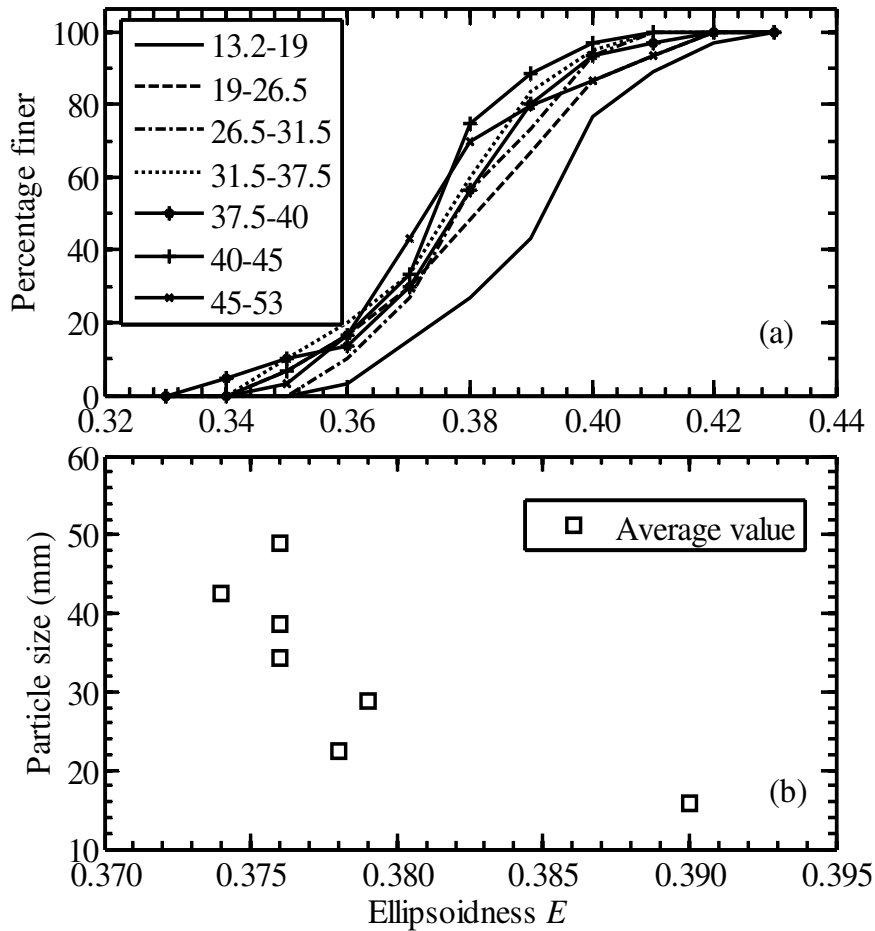
Figure 11. Distribution of ellipsoidness versus (a) percentage finer, and (b) particle size (data sourced from Sun *et al.* [40])

5.   Quantifying particle breakage and implications

Railway tracks are severely influenced by the degradation of ballast particles [33, 43-44]. It is noted that particle breakage under dynamic loads is a complex mechanism that usually begins at the inter-particle contacts (i.e. breakage of asperities), followed by a complete crushing of weaker particles under further loading. A rapid fragmentation of particles and subsequent clogging of voids with fines is commonly observed in overstressed railway foundations. The degradation of particle is the primary cause of contamination, and accounts for up to 40% of the fouled material [45-47]. The main factors that affect ballast degradation can be grouped into three categories: (i) properties related to the characteristics of the parent rock (e.g. hardness, specific gravity, toughness, weathering, mineralogical composition, internal bonding and grain texture); (ii) physical properties related to individual particles (e.g. soundness, durability, particle shape, size, angularity and surface smoothness); and (iii) factors associated with the assembly of particles and loading conditions (e.g. confining pressure, initial density or porosity, thickness of ballast layer, ballast gradation, the presence of water or ballast moisture content, and a cyclic loading pattern including load

amplitude and frequency). Several methods have been used to quantify particle breakage, and some of these indexes are presented in this paper.

Hardin [42] introduced a relative breakage index of $B_r = \dfrac{B_t}{B_p}$ (2)

where, B_t and B_p are the total breakage and breakage potential, respectively. The potential for a particle of soil to break increases with size because the normal contact forces in a soil element increase with particle size, as does the probability of micro-cracks in a given particle increase with its size. Therefore the breakage of particles of soil in a sample of rockfill under moderate stresses will be quite evident, whereas very high stresses are needed to crush silt size particles.

Marsal [9] introduced a breakage index B_g to quantify the breakage of rock-fill materials. His method involves changing the overall grain-size distribution of aggregates after a load has been applied, and carrying out a sieve analysis on specimens before and after each test. From the recorded changes in particle gradation, the difference in percentage retained on each sieve size ($\Delta W_k = W_{ki} - W_{kf}$) is computed, whereby W_{ki} represents the percentage retained on sieve size k before the test and W_{kf} is the percentage retained on the same sieve size after the test. Marsal [9] noticed that some of these differences are positive and some negative; in fact the sum of all positive values of ΔW_k must be theoretically equal to the sum of all negative values. Marsal [9] defined the breakage index B_g as the sum of the positive values of ΔW_k expressed as a percentage, where the breakage index Bg has a lower limit of zero which indicates no particle breakage, and a theoretical upper limit of unity (100%) which represents all the particles broken to sizes below the smallest sieve size used.

Lade *et al.* [48] proposed a new particle crushing parameter with permeability correlations in mind, based on the D_{10} particle size distribution, as given by: $B_{10} = 1 - \dfrac{D_{10f}}{D_{10i}}$ (3)

where, B_{10} = particle breakage factor; D_{10f} = effective grain size of the final gradation; and D_{10i} = effective grain size of the initial gradation. This particle breakage factor is formulated based on the lower limit being zero when there is no particle breakage and the upper limit being unity at infinite particle breakage.

Indraratna *et al.* [18] introduced an alternative ballast breakage index (BBI) based on particle size distribution (PSD) curves. They reported that previous triaxial testing on ballast indicates that particle degradation causes a shift in the initial particle size distribution towards smaller particle sizes, while the maximum size does not change before and after loading. Therefore, instead of defining the breakage potential by a single minute size particle, they considered an arbitrary boundary of maximum breakage which is more appropriate. The ballast breakage index (BBI) is determined on the basis of a change in the fraction which

passes a range of sieves, as shown in Figure 12. This increase in the degree of breakage causes the PSD curve to shift towards the smaller particles size region on a conventional PSD plot, so the area A between the initial and final PSD increases has a larger BBI value; in fact the BBI has a lower limit of 0 (no breakage) and an upper limit of 1. By referring to the linear particle size axis, the BBI can be calculated using the following

equation: $\quad BBI = \dfrac{A+B}{A}$ (4)

where, A is the area defined previously, and B is the potential breakage or area between the arbitrary boundary of maximum breakage and the final particle size distribution.
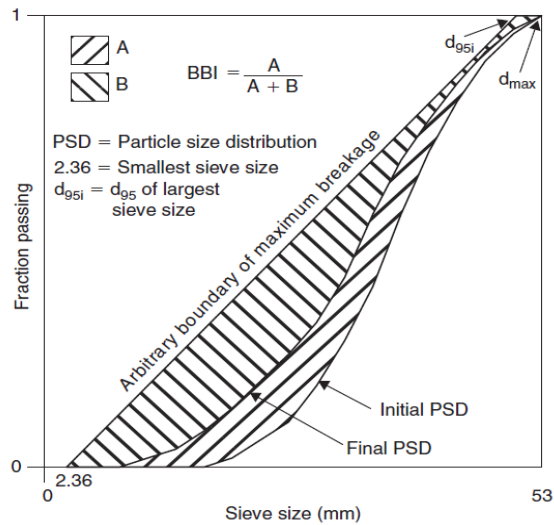

Figure 12. Ballast breakage index (BBI) calculation method (after Indraratna *et al.* [18]).

6. Quantifying ballast fouling

Ballast is a free draining material which contains large void spaces, but as the voids become filled with fouling material track drainage is restricted. Several indices are used in practice to measure the amount of fouling; the fouling index (FI) is defined as the summation of $P_{4.75}$ and $P_{0.075}$, where, $P_{4.75}$ and $P_{0.075}$ are the percentages by mass of material passing the 4.75 mm and 0.075 mm sieve, respectively [1]. The North American Railway systems use typical ballast sizes ranging from 4.76 mm to 51 mm, while Australian Railways uses ballast which varies from 13.2 mm to 63 mm. In view of these differences, the modified Fouling Index (FI_P) is defined as a summation of percentage (by weight) passing the 13.2 mm sieve and 0.075 mm sieve to suit the Australian rail track conditions [2]. A particle size distribution analysis of fouled ballast samples indicates that an intrusion of fines causes significant variations in D_{10} unlike that in D_{90}. Therefore, the modified Fouling Index (FI_D) is defined as the ratio of D_{90} over D_{10} where D_{90} is the particle size corresponding to 90% finer and D_{10} is an effective size [2].

16

However, all the above mass based indices give a false measurement of fouling when the fouling material has a different specific gravity. The Percentage Void Contamination (*PVC*) is expressed by Feldman and Nissen [45] as:

$$PVC = \frac{V_2}{V_1} \times 100$$

(5)

where, V_1 is volume of voids in the ballast and V_2 is the total volume of compacted fouling material. However, in the *PVC* method the volume of fouling material must be calculated after compaction using the standard Proctor method, albeit it does not represent the correct volume of fouling in a real track environment. A better volume based parameter defined as the Void Contaminant Index (VCI) is a reliable estimate of fouling because it includes the effects of the void ratio, specific gravity, and the gradation of fouling material and ballast, as defined by Tennakoon *et al.*[19]; Indraratna *et al.* [24].

$$VCI = \frac{(1+e_f)}{e_b} \times \frac{G_{sb}}{G_{sf}} \times \frac{M_f}{M_b} \times 100$$

(6)

where, e_b is the void ratio of clean ballast, e_f is the void ratio of fouling material, G_{sb} is the specific gravity of ballast material, G_{sf} is the specific gravity of fouling material, M_b is the dry mass of clean ballast, and M_f is the dry mass of fouling material.

As Figure 13 shows, the VCI can capture the amount of fouling better than the other mass based indices because they do not consider the correct volume of fouling in a real track environment. The advantage of VCI is that the volume of mixed fines in comparison with total ballast void volume (e.g. coal and clay) can be captured accurately.
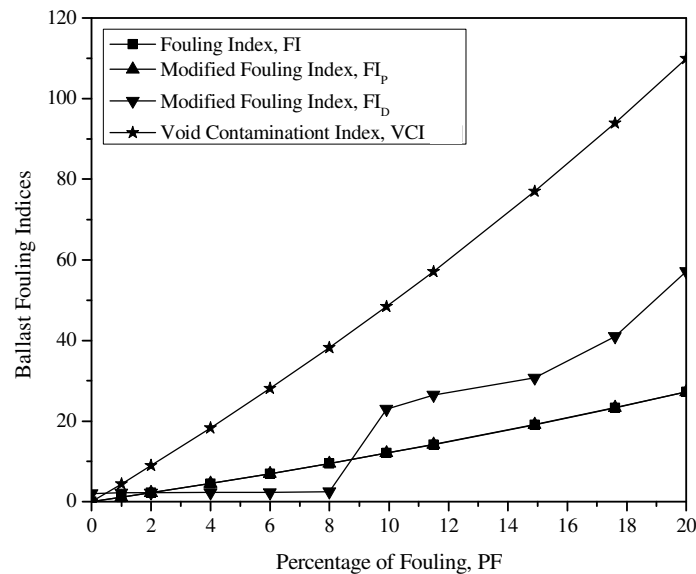

Figure 13. Correlation between fouling indices and *VCI* for various percentages of coal fouling.

7.   Improved performance of fouled ballast using geogrid

This section presents the results of an experimental study of coal-fouled ballast reinforced with geogrid, at various degrees of coal fouling and subjected to cyclic loading. A novel large-scale Process Simulation Testing Apparatus (PSTA) was used to realistically simulate fouled rail track conditions (Figure 14). Details of the PSTA have been described earlier in Section 2. A total of 10 tests were carried out for coal-fouled ballast with and without the inclusion of geogrid, and with a VCI between 0% and 70%. All the tests were carried out at a frequency of 15 Hz with a maximum applied cyclic stress of 420 kPa, and subjected to up to 500,000 load cycles. The ballast was placed in the TPSA and compacted into five layers by a vibratory compactor to a dry density of 1530kg/m^3. A rubber pad was placed beneath the vibrator to prevent particle breakage during compaction. To simulate fouling, a predetermined amount of coal fines were sprayed over each layer to meet the desired VCI. These coal fines then migrated and accumulated into voids between the particles of ballast under gravity and vibration. Every instrument was calibrated before being connected to an electronic DT800 data logger that was controlled by a host computer to accurately record settlements, stress distributions, and lateral movements of the associated walls at pre-determined time intervals.
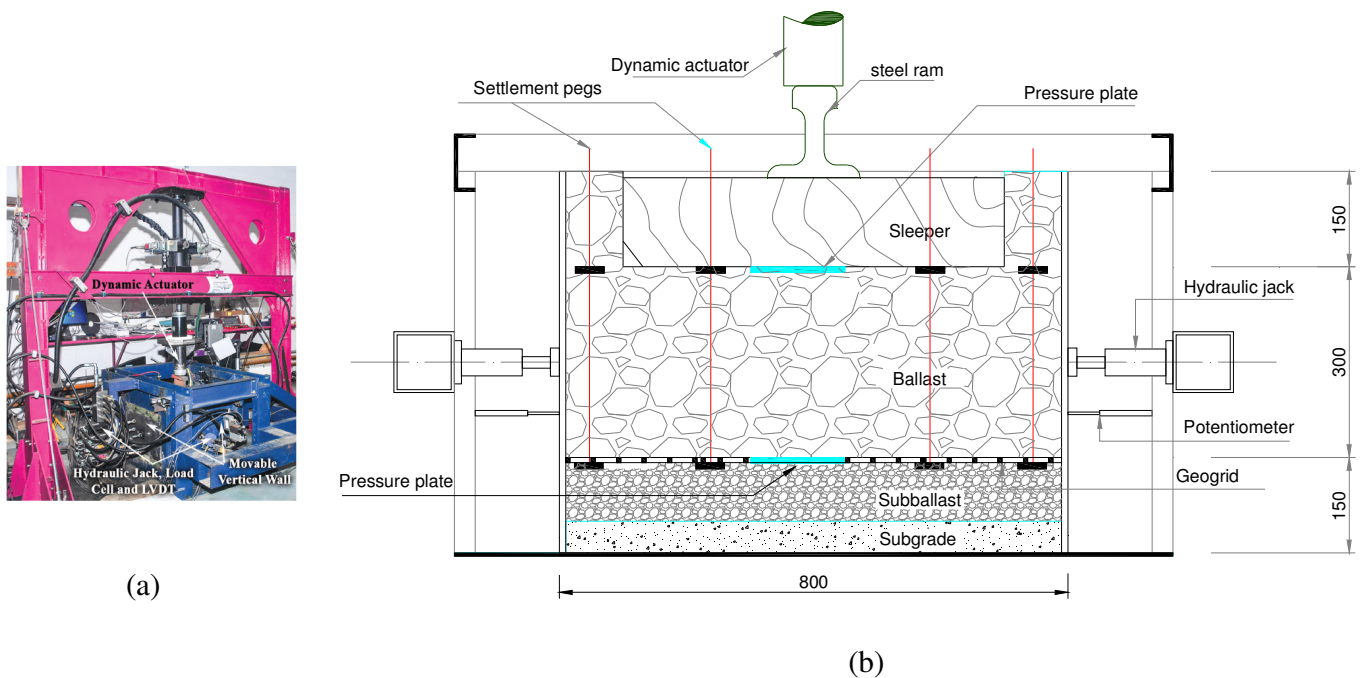

(a)

(b)

Figure 14. (a) Large-scale Process Simulation Testing Apparatus (PSTA); (b) Schematic cross section of the PSTA (after Indraratna *et al.* [20], with permission from ASCE)

Final lateral displacements and vertical settlements of coal-fouled ballast with and without geogrid reinforcement measured in laboratory are presented in Figure 15. It can be seen that the geogrid decreased the lateral displacement of fresh and fouled ballast quite considerably because the ballast created a strong mechanical interlock with the geogrid due to interlocking. This interlocking effect enabled the geogrid to act

as a fixed boundary which reduced deformation. This observation agrees with the previous study by McDowell *et al.* (2006), where the discrete element method (DEM) was adopted to study the interaction between geogrid and ballast. They reported that the geogrid acts like an efficient interlock by forming a stiffened zone inside the ballast assembly. An increased VCI leads to a remarkably higher horizontal displacement and larger settlement. Indeed, when fouling increases, the coal fines would act as a lubricant which assists the particles to slide and/or roll, thereby increase deformation [47]. However, the ability of geogrid to decrease ballast deformation also reduces when the VCI increases because at the end of every test, coal fines had accumulated in the apertures of the geogrids which decreased the effective size of the geogrid aperture. Figure 15d shows the ability of geogrid to reduce the deformation of ballast that is elucidated by the values of a deformation reduction factor, *R*. It is observed that the effect of geogrid became marginal if the VCI exceeded 40%. Indeed, the geogrid performed best when placed in a fresh ballast assembly (approximately 52% and 32% reduction for lateral and vertical deformation, respectively), but it's performed decreased significantly with an increase of VCI (approximately 5% and 12% reduction for lateral and vertical deformation for VCI=40%).
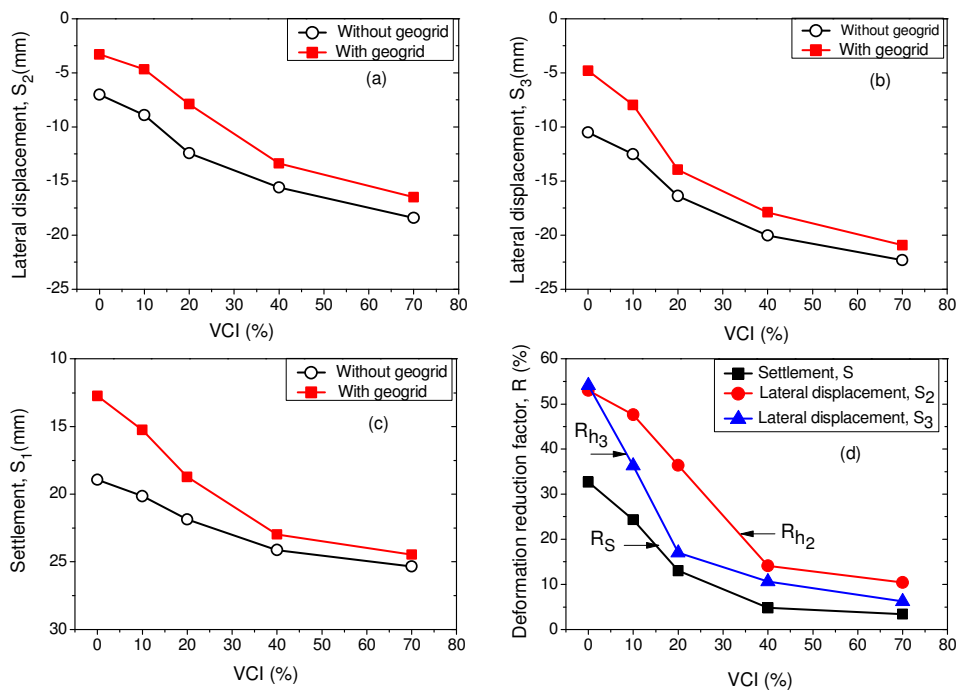

Figure 15. Deformations of fresh and fouled ballast with and without geogrid: (a) lateral displacement S2; (b) lateral displacement S3; (c) settlement S; (d) deformation reduction factor, R (after Indraratna *et al.* [20], with permission from ASCE)

8. Influence of impact forces and benefits of using shock mats

Impact forces occur due to imperfections such as flat wheels, corrugations in the rail, and dipped weld joints. These irregularities are distinct enough to cause the train wheels to impose impact forces on the rail [49]. To

evaluate the effects of these impact forces on ballast deformation and degradation, a series of laboratory tests were carried out using the large scale drop-weight impact testing equipment [27], as shown in Figure 1d. In this test the drop hammer is raised mechanically to the required height and then released by an electronic quick release system to simulate the impact imparted by a typical 'wheel-flat' condition [50]. The impact force imparted by the hammer is measured by a dynamic load cell with a capacity of 1,200 kN, that is mounted at the bottom of the hammer. The impact load was stopped after 10 blows due to an attenuation of strains in the ballast layer. The ability of shock mats to attenuate high frequency impact loads was investigated and a thin layer of compacted sand was used to simulate a typical 'weak' subgrade.

Two distinct force peaks (P_1 and P_2) appeared during impact loading (Figure 16), which was in agreement with a previous study by Jenkins *et al.* [51]. A variation of the P_2 force peak against the number of impact blows is shown in Figure 17. The P_2 force gradually increased as the number of blows increased because the ballast became denser due to the reorientation and rearrangement of aggregates. P_2 increased rapidly at the initial stages of impact loading, but then became almost insignificant. The ballast stabilised after a certain number of impact blows, which resulted in the development of a constant P_2, but even without a shock mat, a ballast layer on a weak subgrade led to a decreased magnitude of P_2 compared to a stiffer subgrade [52].

The ballast was sieved after each test to obtain the BBI, the values of which are presented in Table 1. Only 10 impact blows caused a lot of ballast breakage (i.e. BBI = 17%) when a stiff subgrade was used (Table 1), but when a shock mat was placed above the ballast bed (i.e. under sleeper pad), the BBI decreased by 14.7% for a stiff subgrade and about 23.5% for a relatively weak subgrade, and furthermore, when a shock mat was placed under the ballast mat, the BBI decreased by 31.3% for a stiff subgrade and about 30% for a relatively weak subgrade [50, 52]. In summary, the effectiveness of shock mats depended on where they were placed and the type of subgrade.
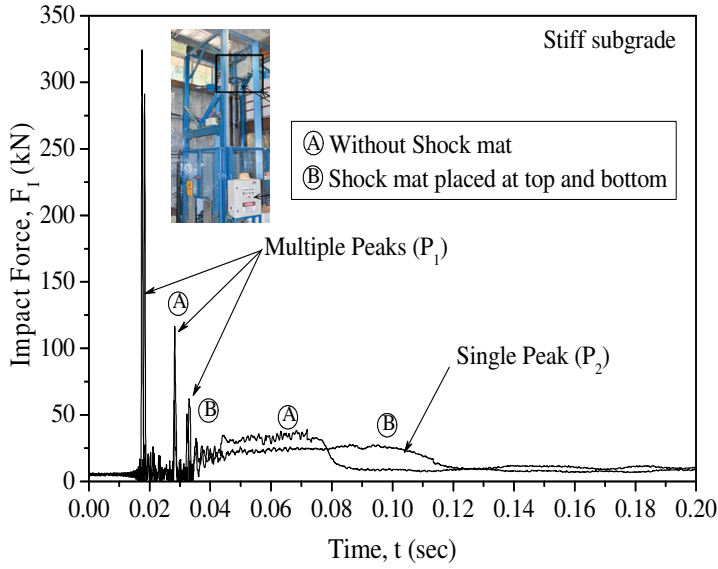
Figure 16. Impact force responses measured in laboratory (after Nimbalkar *et al.* [50], with permission from ASCE)
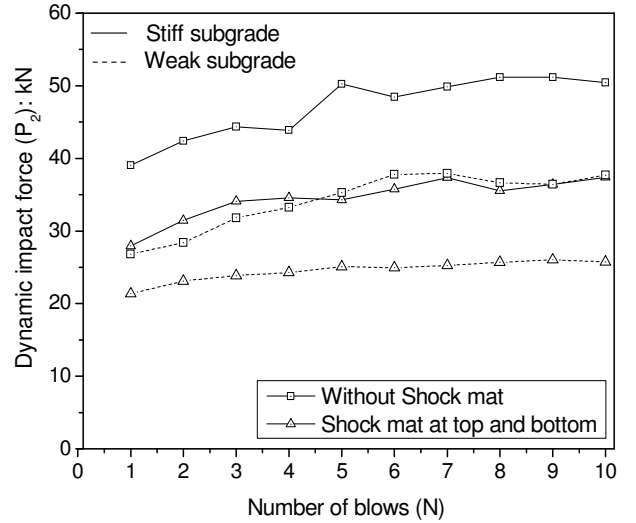
Figure 17. Variation of impact force (P_2) with number of blows (data sourced from Nimbalkar *et al.* [50], with permission from ASCE).

Table 1:   Ballast breakage under impact loading (data source from Nimbalkar *et al.* [50])

Test No.	Base type	Shock Mat Details	*BBI*
1	Stiff	Without shock mat	0.170
2	Stiff	Shock mat at top of ballast (under sleeper pad)	0.145
3	Stiff	Shock mat at bottom of ballast (under ballast mat)	0.130
4	Weak	Without shock mat	0.080
5	Weak	Shock mat at top of ballast (under sleeper pad)	0.055
6	Weak	Shock mat at bottom of ballast (under ballast mat)	0.056

9. Conclusions

This paper presents salient features of the testing method for railway ballast using large-scale ballast testing equipment developed at University of Wollongong with special reference to the deformation and degradation of ballast. It described key research findings in view of the stress-strain responses of ballast subject to static and cyclic loading, as well as the degradation of ballast and its implications on the design and performance of tracks. The influence of confining pressure, particle size distribution, particle angularity, and train speed (frequency) on the degradation and deformation of railroad ballast under cyclic loading has been investigated by large-scale ballast testing apparatus. Cyclic triaxial tests carried out on railway ballast have revealed that particle degradation behavior can be divided into three zones where particle breakage experienced different pattern in these zones. The cyclic triaxial tests conducted in the present study could help to understand the long term response of a railway track under different train speeds where three different deformation mechanisms exist according to frequency (or train speed, V), namely: Range I-Plastic shakedown; Range II-Plastic shakedown and Ratcheting; and Range III-Plastic collapse.

A volume based parameter known as the Void Contaminant Index (VCI) that can capture the extent of fouling better than other mass based indices was considered, and indicated that permanent deformation and degradation increased with the frequency and magnitude of load cycles. A 3D laser scanning method was used to quantitatively assess the size and shape of ballast but then a new shape index called 'ellipsoidness' was introduced to better represent the particle shape index. The large scale triaxial tests revealed that permanent deformation and degradation increased with the frequency and magnitude of load cycles. Three different deformation mechanisms were observed in response to the frequency of loading; in Range I: plastic shakedown at $f \leq 20$ Hz; in Range II: plastic shakedown and ratcheting at 30 Hz $\leq f \leq 50$ Hz; and in Range III: plastic collapse at $f \geq 60$ Hz. The large-scale Process Simulation Testing Apparatus (PSTA) was used to study the load-deformation behavior of coal-fouled ballast reinforced with geogrid, at various degrees of fouling and subjected to cyclic loading. The biaxial geogrid demonstrated their effectiveness by reducing settlement and the movement of particles under cyclic loads. As expected, the geogrid was effective owing to a strong mechanical interlock between the grid apertures and particles of ballast. The large-scale impact tests revealed that impact causes the most damage to ballast, especially under high repetitive loads, although it only takes a few impact blows to cause a lot damage to ballast (i.e. BBI = 17%) with a stiff subgrade.

10.   Acknowledgements

11. References

[1]   Selig, E.T. and Waters, J.M. (1994). Track geotechnology and substructure management, Thomas Telford, London.

[2]   Indraratna, B., Salim, W. and Rujikiatkamjorn, C. (2011a). Advanced Rail Geotechnology - Ballasted Track, CRC Press, Taylor & Francis Group, London, UK

[3]   Tutumluer, E., Huang, H. and Bian, X. (2012). "Geogrid-aggregate interlock mechanism investigated through aggregate imaging-based discrete element modeling approach." *International Journal of Geomechanics*, 12(4), pp: 391-398.

[4]   McDowell, G.R., Lim, W.L., Collop, A.C., Armitage, R. and Thom, N.H. (2008). "Comparison of ballast index tests for railway trackbeds." *Geotechnical Engineering*, 157(3), pp: 151–161.

[5]   Tutumluer, E., Dombrow, W. and Huang, H. (2008). "Laboratory characterization of coal dust fouled ballast behavior." AREMA 2008 Annual Conference & Exposition, Salt Lake City, UT, USA.

[6]   Ngo, N.T., Indraratna, B. and Rujikiatkamjorn, C. (2014). "DEM simulation of the behavior of geogrid stabilised ballast fouled with coal." *Computers and Geotechnics*, 55, pp: 224-231.

[7]   Raymond, G.P. and Diyaljee, V.A. (1979). "Railroad ballast sizing and grading." *Journal of the Geotechnical Engineering Division, ASCE,* 105(GT5), pp: 676-681.

[8]   Ngo, N.T., Indraratna, B. and Rujikiatkamjorn, C. (2017a). "Micromechanics-based investigation of fouled ballast using large-scale triaxial tests and discrete element modeling." *J Geotech Geoenviron Eng*, 134(2), pp: 04016089.

[9]   Marsal R. J. (1967). "Large scale testing of rockfill materials", *Journal of Soil Mechanics and Foundation Engineering, ASCE*, 93(SM2): 27-43.

[10]   Marachi, N.D., Chan, C.K. and Seed, H.B. (1972). "Evaluation of properties of rockfill materials." Soil Mechanics and Foundations Division: Proceedings of the American Society of Civil Engineers, 98(SM1), pp: 95-115.

[11]   Charles, J.A. and Watts, K.S. (1980). "The influence of confining pressure on the shear strength of compacted rockfill." *Geotechnique*, 30(4), pp: 353-367.

[12]   Anderson, W.F. and Fair, P. (2008). "Behavior of railroad ballast under monotonic and cyclic loading." *J Geotech Geoenviron Eng*, 143(3), pp: 316–327.

[13]   Indraratna, B., Ngo, N.T. and Rujikiatkamjorn, C. (2011b). "Behavior of geogrid-reinforced ballast under various levels of fouling." *Geotextiles and Geomembranes*, 29(3), pp: 313-322.

[14]   Indraratna, B., Ionescu, D. and Christie, H. (1998). "Shear behavior of railway ballast based on large-scale triaxial tests." . *J Geotech Geoenviron Eng*, 124(5), pp: 439-449.

[15]   Marsal, R.J. (1973). Mechanical properties of Rockfill. In : Embankment Dam Engineering Wiley, New York, pp: 109-200.

[16]   Ionescu, D. (2004). Evaluation of the engineering behavior of railway ballast. PhD Thesis, University of Wollongong.

[17]   Lackenby, J., Indraratna, B., McDowell, G.R. and Christie, D. (2007). "Effect of confining pressure on ballast degradation and deformation under cyclic triaxial loading." *Geotechnique,* 57(6), pp: 527–536.

[18]   Indraratna, B., Lackenby, J. and Christie, D. (2005). "Effect of confining pressure on the degradation of ballast under cyclic loading." *Géotechnique*, 55(4), pp: 325-328.

[19]   Tennakoon, N., Indraratna, B., Rujikiatkamjorn, C., Nimbalkar, S. and Neville, T. (2012). "The role of ballast-fouling characteristics on the drainage capacity of rail substructure." *ASTM Geotechnical Testing Journal*, 35(4), pp: 1-11.

[20]   Indraratna, B., Ngo, N.T. and Rujikiatkamjorn, C. (2013a). Deformation of coal fouled ballast stabilized with geogrid under cyclic load. . *J Geotech Geoenviron Eng*, 139(8), pp: 1275-1289.

[21]   Rujikiatkamjorn, C., Indraratna, B, Ngo, N.T, and Coop, M. (2012). "A Laboratory Study of Railway Ballast Behavior Under Various Fouling Degree'. Proc., Geosynthetics Asia 2012: 5th

Asian Regional Conference on Geosynthetics, Dec. 13-15, Bangkok, Thailand, 2012, pp. 507-514.

[22]   Biabani, M.M., Indraratna, B. and Ngo, N.T. (2016b). "Modelling of geocell-reinforced subballast subjected to cyclic loading." *Geotextiles and Geomembranes*, 44(4), pp: 489-503.

[23]   Ngo, N.T., Indraratna, B. and Rujikiatkamjorn, C. (2017b). "Simulation Ballasted Track Behavior: Numerical Treatment and Field Application." *International Journal of Geomechanics*, 17(6), pp: 04016130.

[24]   Indraratna, B., Tennakoon, N., Nimbalkar, S. & Rujikiatkamjorn, C. 2013b. Behavior of clay-fouled ballast under drained triaxial testing. *Géotechnique* 63(5): 410-419.

[25]   Biabani, M.M., Ngo, N.T. and Indraratna, B. (2016a). "Performance evaluation of railway subballast stabilised with geocell based on pull-out testing." *Geotextiles and Geomembranes*, 44(4), pp: 579-591.

[26]   Remennikov, A.M. and Kaewunruen, S. (2010) Dynamic crack propagation in prestressed concrete sleepers in railway track systems subjected to severe impact loads. *ASCE-Journal of Structural Engineering*, 136 (6), pp. 749-754.

[27]   Kaewunruen, S. and Remennikov, A.M. (2009). "Progressive failure of prestressed concrete sleepers under multiple high-intensity impact loads". *Engineering Structures*, Vol. 31, No. 10, pp. 2460-2473.

[28]   Ngo, N.T., Indraratna, B. and Rujikiatkamjorn, C. (2016a). "Modelling geogrid-reinforced railway ballast using the discrete element method." *Transportation Geotechnics*, 8(2016), pp: 86-102.

[29]   Australian Standard: AS 2758.7 (1996). Aggregates and rock for engineering purposes; Part 7: Railway ballast. Sydney, NSW, Australia.

[30]   Chrismer, S. M. (1985). Considerations of factors affecting ballast performance, AREA Bulletin AAR Research and Test Dept. Chicago: AAR Technical Centre. Report No. WP-110, pp. 118–150.

[31]   Indraratna B., Wijewardena L.S.S. and Balasubramaniam A.S. (1993). "Large-scale testing of greywacke rockfill", *Geotechnique*, 43(1): 37-51.

[32]   Ramamurthy T. (2001) Shear strength response of some geological materials in triaxial compression. *International Journal of Rock Mechanics and Mining Sciences*, 38, 683–697.

[33]   Sun, Q.D., Indraratna, B. and Nimbalkar, S. (2015). "Deformation and degradation mechanisms of railway ballast under high frequency cyclic loading." *J Geotech Geoenviron Eng*, 142(1), pp: 04015056.

[34]   Ngo, N.T., Indraratna, B., Rujikiatkamjorn, C. and Biabani, M.M. (2016b). "Experimental and discrete element modeling of geocell-stabilised subballast subjected to cyclic loading." *J Geotech Geoenviron Eng*, 142(4), pp: 04015100.

[35]   Altuhafi F, O'Sullivan C, Cavarretta I. (2013). Analysis of an image-based method to quantify the size and shape of sand particles. *J Geotech Geoenviron Eng*.139(8):1290-307.

[36]   Cho G-C, Dodds J, Santamarina JC.(2006). Particle shape effects on packing density, stiffness, and strength: natural and crushed sands. *J Geotech Geoenviron Eng*. 132(5):591-602.

[37]   Le Pen L, Powrie W, Zervos A, Ahmed S, Aingaran S. Dependence of shape on particle size for a crushed rock railway ballast. *Granular Matter*. 2013;15(6):849-61.

[38]   Indraratna, B., Sun, Q.D. and Nimbalkar, S. (2014a). "Observed and predicted behavior of rail ballast under monotonic loadin14,g capturing particle breakage." *Canadian Geotechnical Journal*. 52(1), pp: 73-86.

[39]   Moaveni M, Qian Y, Mishra D, Pombo J. Investigation of ballast degradation and fouling trends using image analysis. Proceedings of 2nd International Conference on Railway Technology, Stirlingshire, UK, Civil-Comp Press. 2014: pp. 1-10.

[40]   Sun Y, Indraratna B, Nimbalkar S.(2014) . Three-dimensional characterisation of particle size and shape for ballast. *Géotechnique Letters*.4(3):197-202.

[41]   O'Sullivan C, Bray JD, Riemer MF. Influence of particle shape and surface friction variability on response of rod-shaped particulate media. *J Eng Mech*. 2002;128(11):1182-92.

[42]   Hardin, B. O. (1985). Crushing of soil particles. *J. of Geotechnical Engineering, ASCE*, Vol. 111, No. 10, pp. 1177-1192.

[43]   Lu, M. and McDowell, G.R. (2006). "Discrete element modelling of ballast abrasion." *Geotechnique,* 56(9), pp: 651-655.

[44]   Indraratna, B., Ngo, N.T., Rujikiatkamjorn, C. and Vinod, J. (2014b). "Behavior of fresh and fouled railway ballast subjected to direct shear testing - a discrete element simulation." *International Journal of Geomechanics, ASCE*, 14(1), pp: 34-44.

[45]   Feldman, F. and Nissen, D. (2002). "Alternative testing method for the measurement of ballast fouling." Conference on Railway Engineering, Wollongong, RTSA.

[46]   Dombrow, W., Huang, H. and Tutumluer, E. (2009). "Comparison of coal dust fouled railroad ballast behavior- granite vs. limestone." Bearing Capacity of Roads, Railways and Airfields, Proceedings of the 8th International Conference (BCR2A'09), Taylor & Francis Group.

[47]   Ngo, N.T., Indraratna, B. and Rujikiatkamjorn, C. (2017c). "Stabilisation of track substructure with geo-inclusions – experimental evidence and DEM simulation." *International Journal of Rail Transportation*, 5(2), pp: 63-86.

[48]   Lade, P.V., Yamamuro, J.A. and Bopp, P.A. (1996). "Significance of particle crushing in granular materials." *Journal of Geotechnical Engineering, ASCE*, 122(4), pp: 309-316.

[49]   Indraratna, B., Nimbalkar, S., Ngo, N.T., and Neville, T. (2016). "Performance improvement of rail track substructure using artificial inclusions - Experimental and numerical studies". *Transportation Geotechnics*.8, pp:69-85

[50]   Nimbalkar, S., Indraratna, B., Dash, S.K. & Christie, D. 2012. Improved performance of railway ballast under impact loads using shock mats. *J. Geotech. Geoenviron. Eng., ASCE* 138(3): 281-294.

[51]   Jenkins, H. M., Stephenson, J. E., Clayton, G. A., Moorland, J. W., and Lyon, D. (1974). "The effect of track and vehicle parameters on wheel/rail vertical dynamic forces." *Railway Engineering Journal*, 3(1), 2–16.

[52]   Nimbalkar, S. and Indraratna, B. (2016). "Improved performance of ballasted rail track using geosynthetics and rubber shockmat." *J Geotech Geoenviron Eng*, 142(8), pp: 04016031.